

Resonant exciton nonlinearities with spatial dispersion

B. F. Levine, R. C. Miller, and W. A. Nordland, Jr.
Bell Laboratories, Murray Hill, New Jersey 07974
 (Received 8 May 1975)

We have measured, using a tunable laser, the resonant second-harmonic generation produced by excitons in CdS and ZnO. We find that spatial-dispersion effects are very important in the harmonic generation, and that only by including them can the data be properly understood. A comparison of the magnitude and sign of the exciton nonlinear coefficient determined from our measurements is found to be in good agreement with theory.

I. INTRODUCTION

For frequencies near the exciton resonance, the large and interesting effects of spatial dispersion on the linear optical properties are well known and have been studied extensively.¹⁻⁵ In contrast, significant effects of the exciton spatial dispersion on the *nonlinear* optical properties have not been clearly demonstrated. For this reason we have performed resonant second-harmonic generation experiments on CdS since the excitons in this crystal are known to be strongly affected by spatial dispersion,^{1,2,5} and further, all the relevant linear exciton parameters are extremely well characterized.^{1,2,5}

Resonant excitonic nonlinearities in CuCl and ZnO were previously investigated in a very nice series of experiments,^{6,7} but since the Bohr radii for excitons in these materials are small, spatial-dispersion effects are expected to be small.^{8,9} In fact, a good fit to the CuCl second-harmonic generation data^{6,7} was possible using a classical expression which completely neglected spatial dispersion. However, the Bohr radius for excitons in^{1,5} CdS is four times larger than that for CuCl.⁸

Another factor which prompted our measurement of CdS is that it has a *positive*¹⁰ second-harmonic coefficient $d_{333} > 0$, whereas both CuCl and

ZnO have *negative*¹⁰ coefficients, i.e., $d_{123}(\text{CuCl}) < 0$ and $d_{333}(\text{ZnO}) < 0$. A previous theoretical treatment¹¹ for the exciton contribution to d_{ijk} was successful in calculating the selection rules, magnitude, and absolute sign for CuCl and ZnO, and it was suggested¹¹ that a strong test of the predictions of this theory would be the measurement of a crystal possessing a positive d_{ijk} such as CdS.

II. EXPERIMENTAL

A schematic diagram of the experimental apparatus is shown in Fig. 1. The tunable fundamental frequency (near $\lambda \sim 1 \mu\text{m}$) was generated by a Chromatix laser which pumps a parametric oscillator, whose output was tuned so that the second-harmonic frequency generated in the accentric crystal (e.g., CdS or ZnO) was swept through the exciton resonance. The parametric oscillator had a linewidth of $\sim 1 \text{ cm}^{-1}$ at the fundamental (i.e., $\sim 0.25 \text{ \AA}$ at the harmonic) and an absolute wavelength calibration with an uncertainty of $\pm 5 \text{ \AA}$. However, the relative wavelength scale for a sweep across the exciton resonance was at least an order of magnitude more accurate. The amplitude stability of the oscillator which was operated at 50 pulses/sec was $\pm 20\%$. Because of the large resonant changes ($\sim 10^3$) in the generated harmonic power,

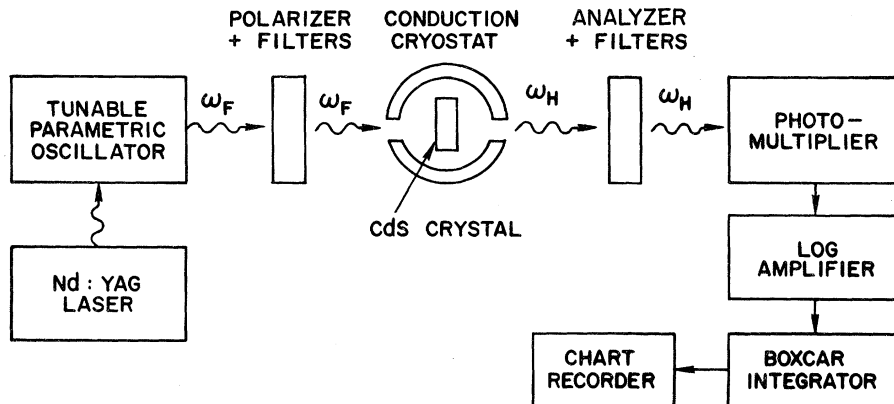


FIG. 1. Schematic of the experimental apparatus for the measurement of resonant exciton second-harmonic generation.

a logarithmic amplifier was used before the boxcar integrator. At the very smallest signal levels ($\sim 10^{-3}$ of the phase-matched harmonic peak) the nonlogarithmic response of the amplifier was corrected for.

In these experiments, it was necessary to cool the crystals, and therefore they were mounted on the cold finger of a helium Dewar (resulting in a sample temperature of $\sim 10^\circ\text{K}$). The two CdS crystals were platelets (17 and 25 μm thick) with the hexagonal c axis in the plane of the samples. Microscopic examination of the as-grown crystals revealed regions that were highly perfect on the surface and throughout the volume. The measured linear reflectivity as a function of wavelength was identical to that reported in the literature^{1,2,5} with the usual anomalous spikes due to spatial dispersion. This further demonstrates the quality and perfection of these crystals.

In the case of CdS the oscillator output was focused into the sample with a 2.5-cm focal length lens, and the generated harmonic collected with a 7.5-cm focal length lens. For ZnO these two lenses were 7.5 and 25 cm, respectively. In both cases a 2-cm path length of CuSO_4 saturated in water was used to help eliminate the fundamental from the detector system. In order to cut down on the two-photon-induced fluorescence from ZnO, the detector and associated filters were placed about 120 cm from the sample.

Some of the experimental data for the second-harmonic power generated as the harmonic was swept through the exciton resonance are shown in Figs. 2-4. The data for CdS show the Maker fringe oscillations¹² as the frequency increases toward the exciton resonance ω_0 . This is a result of the rapidly increasing refractive index at the harmonic frequency as ω_0 is approached. Note that owing to the increasing absorption, the amplitude of the fringes decreases and they disappear altogether $\sim 10 \text{ \AA}$ below the CdS A- and B-

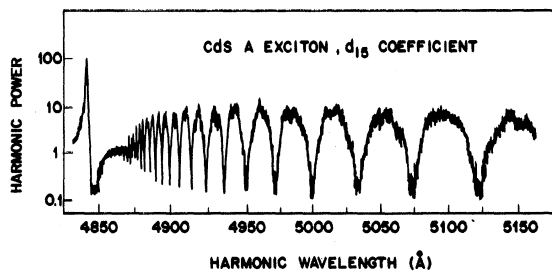


FIG. 2. Experimental second-harmonic power as a function of harmonic wavelength for the CdS d_{15} coefficient. Maker fringes are clearly evident as is the large resonant exciton nonlinearity near 4840 \AA .

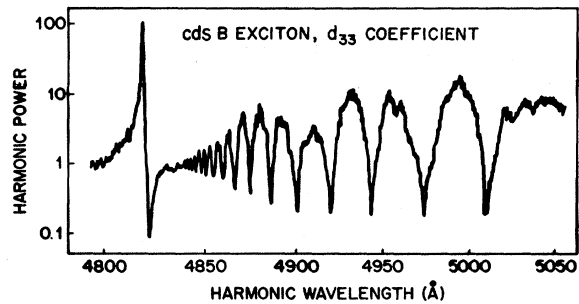


FIG. 3. Experimental second-harmonic power as a function of harmonic wavelength for the CdS d_{33} coefficient.

exciton resonances. Owing to the large absorption in ZnO the Maker fringes only appear far away from the exciton resonance frequency. Although Haueisen and Mahr⁶ studied ZnO previously, they did not investigate the A exciton [shown in Fig. 4], apparently because they thought this exciton was

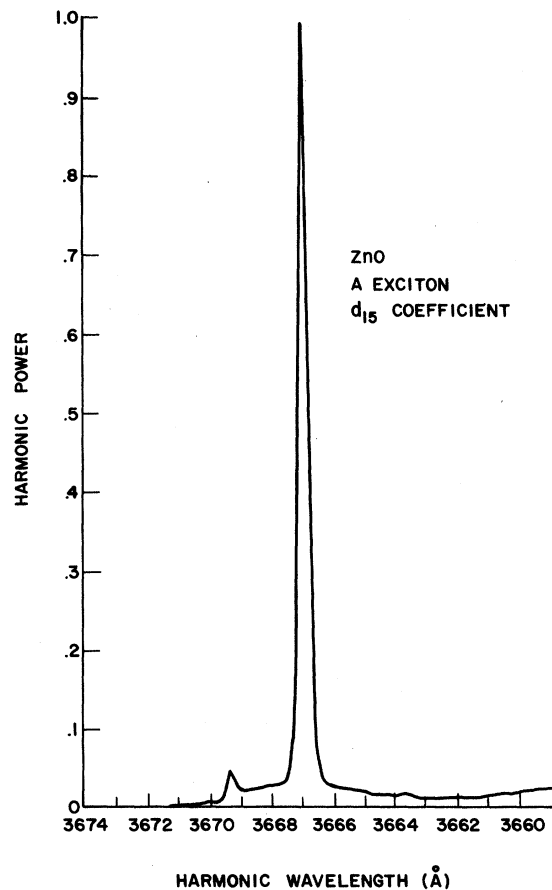


FIG. 4. Experimental second-harmonic power as a function of harmonic wavelength for the ZnO d_{15} coefficient. Large peak at 3667 \AA is due to phasematching.

forbidden by symmetry. The large peaks in the harmonic intensity shown in Figs. 2-4 are due to the phase matching of the nonlinear process as the linear index changes rapidly near the exciton resonance.

III. SELECTION RULES

By properly adjusting the polarizer and analyzer, the harmonic generated by each of the exciton nonlinear coefficients d_{ijk}^{ex} was investigated, and the results showing which nonlinearities were observed experimentally are given in Table I. The expected selection rules are determined from¹¹

$$d_{ijk}^{\text{ex}} \propto \alpha_{ii} d_{ijk}^{\text{el}}, \quad (1)$$

where α_{ii} is the linear exciton polarizability for light polarized along the i principal axis, and d_{ijk}^{el} is the usual electronic nonlinear coefficient. Thus, the first requirement¹¹ for the existence of d_{ijk}^{ex} is that $d_{ijk}^{\text{el}} \neq 0$, i.e., the exciton nonlinear coefficient must satisfy all the usual crystal symmetry requirements. Thus, for example, $d_{111}^{\text{ex}} = 0$ for CdS and ZnO which have the wurtzite structure. In addition, the linear exciton polarizability α_{ii} (i.e., the exciton oscillator strength) must not vanish¹¹ for light polarized in the direction expected for the second-harmonic polarization. As an example, consider the A exciton in CdS. The coefficient d_{113} is allowed but d_{311} is forbidden, since the A -exciton oscillator strength is polarized perpendicular to the c axis. Thus, this selection rule ($d_{113} \neq 0$ but $d_{311} = 0$), of course, strongly violates Kleinman symmetry,^{10, 13} which might have been expected owing to the close proximity of a resonance.^{14, 15} As shown in Table I, the expected selection rules for CdS and ZnO are obeyed except perhaps for the ZnO C exciton, near which little structure is observed.

It should be noted in this regard that even though a nonlinear coefficient d_{ijk}^{ex} is allowed, it is possible that little or no structure will be evident near the phase-matching frequency. This can occur if the position of the minimum in the generated harmonic power (due to the destructive interference between d_{ijk}^{ex} and d_{ijk}^{el}) is so close to the phase-matched harmonic peak that the damping is large enough to wash out any sharp structure. This is in fact the case for the C exciton in ZnO since neither our measurements nor those of Haueisen and Mahr⁶ revealed any strong structure near this resonance.

IV. CLASSICAL ANALYSIS

In this section we neglect spatial dispersion and treat the harmonic production completely clas-

sically^{6, 7} to illustrate the importance of the spatial dispersion on the harmonic generation process in CdS. The linear frequency-dependent optical dielectric constant $\epsilon(\omega) = n(\omega)^2$ [where $n(\omega)$ is the index of refraction] is simply given by

$$\epsilon_{ii}(\omega) = \epsilon_{ii}^0 + 4\pi\alpha_{ii}\omega_0^2/(\omega_0^2 - \omega^2 - i\omega\Gamma), \quad (2)$$

where ϵ^0 is the background dielectric constant, i.e., the value which would be appropriate if the exciton polarizability α were zero, ω_0 is the exciton resonant frequency, and Γ is the damping constant. For CdS the values for these classical parameters are well known from measurements of the reflectivity spectra^{1, 2, 5} and are, for the A exciton,

$$\begin{aligned} \omega_0 &= 2.5528 \text{ eV}, \quad \epsilon_{xx}^0 = 8.1, \\ 4\pi\alpha_{xx} &= 9.4 \times 10^{-3}, \quad \Gamma = 1.0 \times 10^{-3} \text{ eV}, \end{aligned} \quad (3)$$

while for the B exciton these parameters are

$$\begin{aligned} \omega_0 &= 2.5679 \text{ eV}, \quad \epsilon_{xx}^0 \approx \epsilon_{zz}^0 = 8.1, \\ 4\pi\alpha_{xx} &\approx 4\pi\alpha_{zz} = 5.6 \times 10^{-3}, \quad \Gamma = 1.0 \times 10^{-3} \text{ eV}. \end{aligned} \quad (4)$$

Thus, using $\epsilon(\omega) = [\tilde{n}(\omega)]^2$, where the classical complex refractive index is given by $\tilde{n}(\omega) = n(\omega) + ik(\omega)$, the frequency-dependent values for the real and imaginary parts of the refractive index are readily obtained from Eq. (2).

The classical frequency dispersion of the nonlinear susceptibility at $\omega_H = 2\omega_F$ is given by an expression similar to Eq. (2), namely⁶

TABLE I. Comparison of experimentally observed resonant exciton contributions to a particular nonlinear coefficient d_{ijk} , and those expected from the selection rule Eq. (1).

Crystal	Exciton	Coefficient	(observed)	Selection rule
CdS	A	d_{113}	(Yes)	Allowed
CdS	A	d_{311}	(No)	Forbidden
CdS	A	d_{333}	(No)	Forbidden
CdS	B	d_{113}	(Yes)	Allowed
CdS	B	d_{311}	(Yes)	Allowed
CdS	B	d_{333}	(Yes)	Allowed
ZnO	A	d_{113}	(Yes)	Allowed
ZnO	A	d_{311}	(No)	Forbidden
ZnO	A	d_{333}	(No)	Forbidden
ZnO	C	d_{113}	(No)	Forbidden
ZnO	C	d_{311}	(No)	Allowed
ZnO	C	d_{333}	(No)	Allowed

$$d_{ijk}(\omega_H) = d_{ijk}^{el} + d_{ijk}^{ex} \omega_0^2 / (\omega_0^2 - \omega_H^2 - i\omega_H \Gamma), \quad (5)$$

where d_{ijk}^{el} is the background electronic nonlinear coefficient, and where d_{ijk}^{ex} is the exciton contribution.

Having expressions for the linear and nonlinear susceptibilities we can now calculate the frequency dependence of the second-harmonic intensity I_{shg} ,^{6, 12}

$$I_{shg}(\omega_H) \propto \frac{|d_{ijk}(\omega_H)|^2}{|\tilde{n}(\omega_H) - n(\omega_H)|^2 |\tilde{n}(\omega_H) + 1|^2}, \quad (6)$$

where we have used the fact that near the resonance the absorption constant α_{abs} is so large that $\alpha_{abs} t \gg 1$, (where t is the crystal thickness). Since the only unknown in Eq. (6) is d_{ijk}^{ex} (contained in d_{ijk}), it can be readily determined by a fit to our second-harmonic resonance measurements. The best fit using the known linear parameters already mentioned above is obtained with

$$d_{333}^{ex} / d_{333}^{el} = +1.7 \times 10^{-3}, \quad (7)$$

as shown in Fig. 5. The agreement with experiment is poor. The classical calculation predicts the harmonic generation at the phase-matching peak ($\lambda = 4821 \text{ \AA}$) to be a factor of ~ 25 too low.

V. SPATIAL DISPERSION

A. Linear effects

We saw that the classical fit for CdS to the second-harmonic measurements was very poor. This is in marked contrast to the previously considered cases^{6, 7} of CuCl and ZnO. However, the failure of the classical approach for CdS should not really be too surprising since it is well known, owing to the large exciton radius, that linear spatial dispersion is very important in this material.^{1, 2, 5} Thus, we now consider the effects of spatial dispersion on the generation of the harmonic field.

One of the major effects of the spatial dispersion is the introduction of an additional mode, so that now two propagating transverse modes exist (in each direction) for a given principal polarization and frequency.¹ Each of these two waves will generate harmonics which will interfere and thus significantly affect the net harmonic power. The fact that there are two propagating modes can be easily seen from the form¹ of the dielectric constant $\epsilon(k, \omega)$:

$$\epsilon_{ii}(k, \omega) = n_i^2(k, \omega) = \epsilon_{ii}^0 + 4\pi\alpha_{ii} \omega_0^2 / (\omega_k^2 - \omega^2 - i\omega\Gamma). \quad (8)$$

The difference between this spatial dispersion relation and the classical relation Eq. (2), is that the exciton resonance frequency ω_k is k dependent.

This dependence can be expressed as¹

$$\hbar\omega_k = \hbar\omega_0 + \hbar^2 k^2 / 2m^*, \quad (9)$$

where ω_0 is the frequency without spatial dispersion (i.e., at $k=0$), and where m^* is the exciton mass. Clearly as m^* approaches infinity, the importance of spatial dispersion vanishes. The refractive indices for the two modes are readily obtained by eliminating k in Eq. (8) using $k = \pm n\omega/c$. The result for the two solutions are¹

$$\begin{aligned} n^2 &= [\frac{1}{2}(\epsilon_0 - \Omega\mu)] \pm \{[\frac{1}{2}(\epsilon_0 + \Omega\mu)]^2 + 4\pi\alpha\mu\}^{1/2}, \\ \Omega &\equiv 1 - \omega^2/\omega_0^2 - i\Gamma\omega/\omega_0^2, \\ \mu &\equiv m^*c^2\omega_0/\hbar\omega^2, \end{aligned} \quad (10)$$

where Ω and μ are the dimensionless frequency and mass, respectively.

By solving the optical reflectivity problem using the exciton "dead layer" boundary condition¹⁻⁵ (which we will discuss in more detail below), and fitting the experimental frequency-dependent reflectivity curves, Hopfield and Thomas¹ have determined all the relevant linear exciton parameters when spatial dispersion is included. These were found to be¹ for the A exciton

$$\begin{aligned} \epsilon^0 &= 8.0, \quad \omega_0 = 2.5528 \text{ eV}, \\ 4\pi\alpha &= 12.5 \times 10^{-3}, \quad \Gamma = 1.0 \times 10^{-4} \text{ eV}, \\ m^* &= 0.9m_0, \quad l = 100 \text{ \AA}, \end{aligned} \quad (11)$$

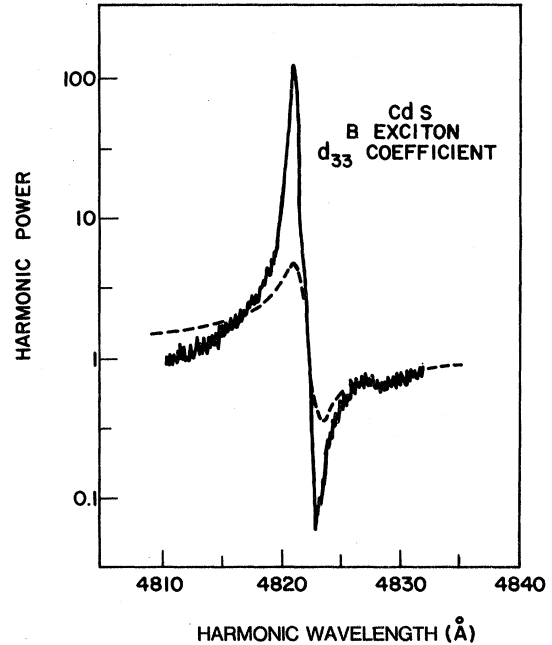


FIG. 5. Comparison of experimental resonant second-harmonic power for the CdS B exciton (solid curve) with a theoretical fit neglecting spatial dispersion (dashed line).

where m_0 is the free electron mass and l is the dead layer depth. The parameters for the B exciton are^{1,2}

$$\begin{aligned} \epsilon^0 &= 8.0, \quad \omega_0 = 2.5679 \text{ eV}, \\ 4\pi\alpha &= 7.5 \times 10^{-3}, \quad \Gamma = 1.0 \times 10^{-4} \text{ eV}, \\ m^* &= 1.3m_0, \quad l = 100 \text{ \AA}. \end{aligned} \quad (12)$$

The most striking and important difference between the classical and spatial dispersion parameters is the order of magnitude larger damping in the classical case, i.e., Γ is 10^{-3} and 10^{-4} eV for the classical and spatial dispersion cases, respectively. This arises since for the classical exciton, damping is the only quantity which reduces the reflectivity peak from 100%. However, when spatial dispersion is present the finite exciton mass $m^* \neq \infty$ is mostly responsible for the reduction of the reflectivity peak.¹ Thus, neglecting spatial dispersion and fitting the reflectivity classically can result in an artificially large damping parameter Γ , and hence a predicted value for the second-harmonic power at phase matching which is too low. This may be part of the reason that nonlinear determinations^{6,7} of Γ are significantly smaller than those obtained from linear reflectivity measurements [i.e., using Eq. (2)]. As we will see later, by correctly including the effects of spatial dispersion, all of the exciton parameters necessary for fitting the harmonic generation (except of course for d^{ex}) can be taken directly from linear reflectivity determinations.^{1,2}

Before proceeding to a determination of d_{ijk}^{ex} , the Maker fringes for the CdS A and B excitons (shown in Figs. 2 and 3) provide an opportunity to check the value of the linear exciton polarizability α de-

termined by reflectivity measurements.^{1,2} From our measurements of the second-harmonic Maker fringe spacing, we can obtain the dispersion in the refractive index near ω_0 and compare it with that expected from Eq. (8). It is easy to show that the increase in index $n(\omega)$, as the wavelength $\lambda = 2\pi c/\omega$ is decreased, is given by

$$n(\omega) = n_0 + N\lambda/t, \quad (13)$$

where N is an integer which labels the successive fringes, n_0 is the value of the index for $N=0$ [not the same as the low-frequency limit $n(0)$], and t is the crystal thickness. Thus, for example, the A exciton of CdS (shown in Fig. 2) for which $t = 25 \mu\text{m}$, has a difference in index Δn from one Maker fringe to another of $\Delta n = \lambda/t \sim 0.02$.

Before comparing the experimental [Eq. (13)] and calculated [Eq. (8)] values of $n(\omega)$, it is important to note that the background value ϵ^0 is not really a constant. It has a weak frequency dependence due to the main dispersion of the electronic resonance in the ultraviolet. This weak dispersion only changes ϵ^0 by less than 1% over the narrow width of the exciton resonance ($\Delta\lambda \sim 10 \text{ \AA}$), and can therefore be accurately assumed constant when fitting data over this restricted frequency region. However, our Maker fringe data cover several hundred angstroms and are sufficiently accurate that the weak dispersion of ϵ^0 must be included to achieve a precise fit to the data. We have fitted ϵ^0 to experiment (using a standard single oscillator resonance expression) for frequencies far enough from the exciton ω_0 so that its contribution is negligible, but close enough to the band gap so that the dispersion of ϵ^0 near ω_0 can be accurately determined; that is about 500 \AA away from

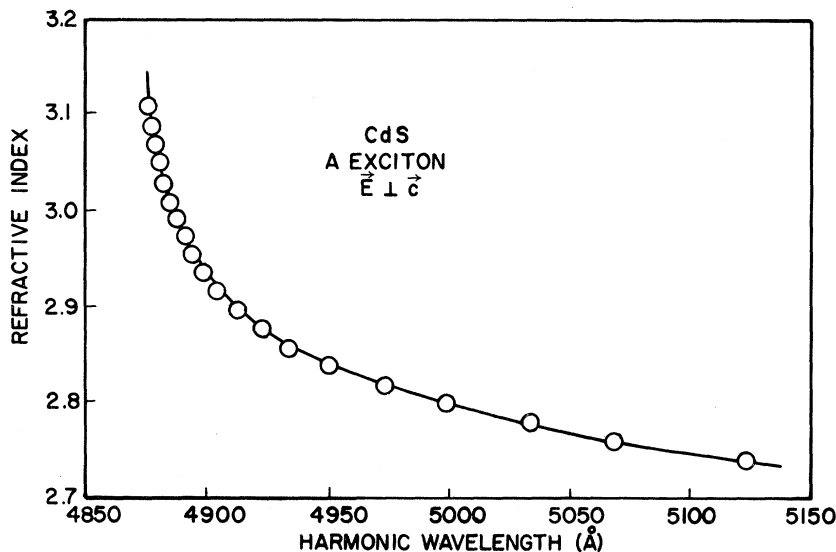


FIG. 6. Comparison of the refractive index of the CdS A exciton determined from our measurements of the Maker fringe minima (open circles) and that calculated using the known spatial dispersion parameters (solid line).

ω_0 . The excellent fit of Eq. (8) (using the linear parameters given previously) to our data is shown for the *A* and *B* excitons of CdS in Figs. 6 and 7. The only adjustable parameter is the constant n_0 in Eq. (13). This is unknown since the Maker fringe separations only determine the index differences Δn . The good agreement shown in Figs. 6 and 7 indicates that the linear parameters in the spatial dispersion susceptibility [Eq. (10)] obtained from reflectivity measurements^{1,2} accurately describe our transmission experiments. The fit to the *B* exciton is not quite as good as that for the *A* exciton and may be related to the significantly smaller value of the *B*-exciton polarizability, and the increased importance of the background dispersion ϵ^0 . A similar comparison of our Maker fringe data using the classical exciton parameters [i.e., Eqs. (3) and (4)] is significantly (~30%) worse.

B. Nonlinear susceptibility—CdS

In order to fit the experimental second-harmonic intensity we need to derive the effects of spatial dispersion on both the nonlinear coefficient d_{ijk}^{ex} as well as its effect on the harmonic generation and propagation. Because of the spatial dispersion there will be, as mentioned before, two propagating modes having different indices n_1 and n_2 given by the two solutions to Eq. (10). These two modes will satisfy the nonlinear wave equation

$$-k_\sigma^2 E_\sigma + (n_\sigma \omega_H/c)^2 E_\sigma = -4\pi(\omega_H/c)^2 P_\sigma^{nl}, \quad (14)$$

$$P_\sigma^{nl} = d_\sigma E_F^2, \quad (15)$$

where the mode index σ labels the particular mode (say 1 or 2), k_σ is the propagation constant of the particular mode, n_σ is one of the two index solutions to Eq. (10), E_σ is the mode harmonic field, $\omega_H = 2\omega_F$ is the harmonic frequency, P_σ^{nl} is the nonlinear polarization produced by the total (exciton plus electron) nonlinear coefficient, $d_\sigma = d^{el} + d_\sigma^{ex}$, and E_F is the fundamental field amplitude (for notational simplicity tensor indices such as those on d_{ijk} have been suppressed). The solution to Eq. (14) is well known¹² to be

$$E_\sigma(x) = A_\sigma e^{ik_\sigma x} + B_\sigma e^{ikx}, \quad (16)$$

where the first term arises from the homogeneous solution to Eq. (14) (usually called the free wave) and has a wave vector

$$k_\sigma = n_\sigma \omega_H/c. \quad (17)$$

The second term is the driven or bound wave having a wave vector

$$k = n_F \omega_H/c, \quad (18)$$

where n_F is the index at the fundamental frequency ω_F , and has an amplitude

$$B_\sigma = 4\pi d_\sigma E_F^2 / (n_\sigma^2 - n_F^2), \quad (19)$$

$$d_\sigma = d^{el} + d^{ex} \omega_0^2 / [(\omega_k)_\sigma^2 - \omega^2 - i\omega\Gamma], \quad (20)$$

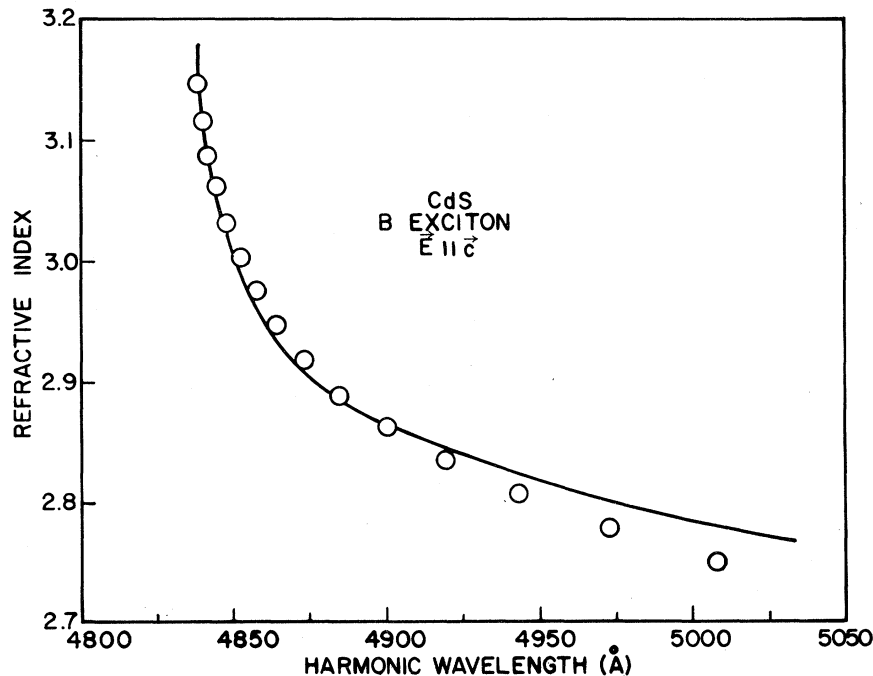


FIG. 7. Comparison of the refractive index of the CdS *B* exciton determined from our measurements of the Maker fringe minima (open circles) and that calculated using the known spatial dispersion parameters (solid line).

where $(\omega_k)_\sigma$ is given by Eq. (9), i.e.,

$$(\hbar\omega_k)_\sigma = \hbar\omega_0 + \hbar^2 k_\sigma^2 / 2m^* . \quad (21)$$

We now have to solve the boundary problem illustrated in Fig. 8. The exit face of the crystal is shown with a "dead layer" of thickness l in which the exciton cannot propagate, i.e., the exciton polarization must drop to zero at a distance l from the surface,^{1, 16} and the nonlinear coefficient is simply d^{el} in this "dead layer."

Thus, the total field E_i incident on the dead layer at $x=0$ is

$$E_i(x) = E_1(x) + E_2(x) , \quad (22)$$

with E_1 and E_2 given by Eq. (16). Because we are interested in frequencies near the exciton resonance where the absorption is very strong, the free wave term in Eq. (16) which propagates with the complex refractive index n_σ , will be highly absorbed and can be neglected. This can be readily seen experimentally in Fig. 2 where the Maker fringe interference pattern between the free and bound waves of Eq. (16) disappears as the exciton resonance is approached, and the free wave is absorbed. Thus, the incident wave is simply

$$E_i(x) = (B_1 + B_2) e^{ikx} , \quad (23)$$

while to a good approximation the other fields are given by

$$E_r(x) = A_1 e^{-ik_1 x} + A_2 e^{-ik_2 x} , \quad (24)$$

$$E_t(x) = A_0 e^{ik_0 x} + B_0 e^{ikx} , \quad (25)$$

$$E_r'(x) = A' e^{-ik_0 x} , \quad (26)$$

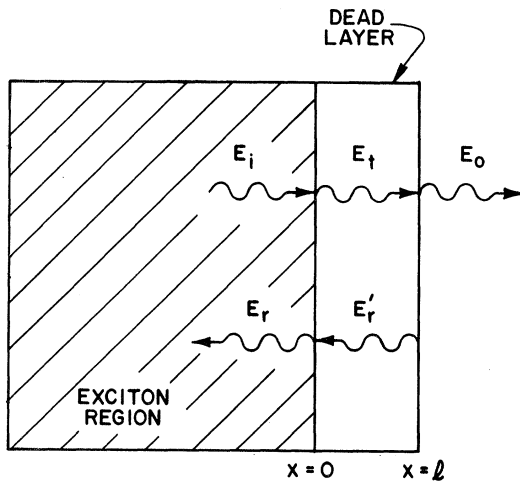


FIG. 8. Incident, transmitted, and reflected fields near the exit face of the nonlinear crystal showing the bulk region (shaded) where exciton propagation exists and the dead layer from $x=0$ to $x=l$ (of order a few Bohr radii) from which the exciton is excluded.

where $k_1 = n_1 \omega_H / c$ [from Eq. (17)], $k_0 = n_H^0 \omega_H / c$, n_H^0 is the background index at the harmonic frequency with no exciton contribution, i.e., $n_H^0 = \sqrt{\epsilon^0}$, and where

$$B_0 = 4\pi d^{\text{el}} E_F^2 / [(n_H^0)^2 - n_F^2] . \quad (27)$$

Thus, matching boundary conditions at $x=0$ we find, using the usual continuity relations for the electric and magnetic fields,

$$B_1 + B_2 + A_1 + A_2 = A_0 + B_0 + A' , \quad (28)$$

$$n_F B_1 + n_F B_2 - n_1 A_1 - n_2 A_2 = n_H^0 A_0 + n_F B_0 - n_H^0 A' . \quad (29)$$

The other boundary condition we need is that the total exciton polarization vanishes at the "dead layer" boundary¹ $x=0$, i.e.,

$$(n_1^2 - \epsilon^0) A_1 + (n_2^2 - \epsilon^0) A_2 = 0 . \quad (30)$$

The boundary conditions at $x=l$ are simply

$$A_0 e^{ik_0 l} + B_0 e^{ikl} + A' e^{-ik_0 l} = E_0 , \quad (31)$$

$$n_H^0 A_0 e^{ik_0 l} + n_F B_0 e^{ikl} - n_H^0 A' e^{-ik_0 l} = E_0 . \quad (32)$$

The harmonic intensity generated can now be obtained from

$$I_{\text{shg}}(\omega_H) \propto |E_0|^2 , \quad (33)$$

where

$$E_0 = [(2n_H^0)/(n_H^0 + 1)] E_{\text{ex}} e^{i\Delta k l} + [(n_H^0 + n_F)/(n_H^0 + 1)] B_0 , \quad (34)$$

$$\Delta k = k_0 - k = (n_H^0 - n_F) (\omega_H / c) , \quad (35)$$

$$E_{\text{ex}} = (C_F B e^{-2ikl} - D_F B_0 e^{i\Delta k l}) / (C_H e^{-2ikl} - D_H e^{2i\Delta k l}) , \quad (36)$$

$$B = B_1 + B_2 - B_0 , \quad (37)$$

with B_1 and B_2 given by Eq. (19), B_0 given by Eq. (27) and

$$C_F = \frac{[n_1^2 - (n_H^0)^2](n_2 + n_F) - [n_2^2 - (n_H^0)^2](n_1 + n_F)}{[n_1^2 - (n_H^0)^2](n_2 - n_H^0) - [n_2^2 - (n_H^0)^2](n_1 - n_H^0)} , \quad (38)$$

$$C_H = \frac{[n_1^2 - (n_H^0)^2](n_2 + n_H^0) - [n_2^2 - (n_H^0)^2](n_1 + n_H^0)}{[n_1^2 - (n_H^0)^2](n_2 - n_H^0) + [n_2^2 - (n_H^0)^2](n_1 - n_H^0)} , \quad (39)$$

$$D_F = (n_F - 1)/(n_H^0 + 1); \quad D_H = (n_H^0 - 1)/(n_H^0 + 1) . \quad (40)$$

In the limit of weak spatial dispersion these complicated expressions go over correctly to the classical limit. That is, setting $d^{\text{ex}} = 0$, $l = 0$, $n_1 \rightarrow n_H^0$, and $n_2 \rightarrow \infty$ results in

$$I_{\text{shg}}(\omega_H) \propto (d^{\text{el}})^2 / (n_H^0 - n_F)^2 (n_H^0 + 1)^2, \quad (41)$$

which is exactly the classical result Eq. (6). Since all the linear exciton parameters have already been determined,^{1,2} the only unknown in Eq. (33) is d_{ijk}^{ex} . By varying d_{ijk}^{ex} to achieve the best fit to our resonant second-harmonic generation data, we can readily determine d_{ijk}^{ex} . (Owing to our $\pm 5 \text{ \AA}$ calibration uncertainty, it was necessary to adjust the experimental data on the CdS *A* and *B* excitons by $\sim 3 \text{ \AA}$.) The results of a computer fit of Eq. (33) are shown for the *A* and *B* excitons of CdS in Figs. 9 and 10, and the best-fit values of d_{ijk}^{ex} are given in Table II. Note that while the best-fit value for the *B* exciton,

$$d_{113}^{\text{ex}}/d_{113}^{\text{el}} = 1.7 \times 10^{-3}, \quad (42)$$

is the same as that for the classical case, Eq. (7), the over-all fit including spatial dispersion is far superior. In particular, the spatial dispersion theory correctly predicts the large magnitude of the phase-matched harmonic peak, whereas the classical prediction was 25 times too small.

The minimum of the *A*-exciton experimental data (caused by the destructive interference between

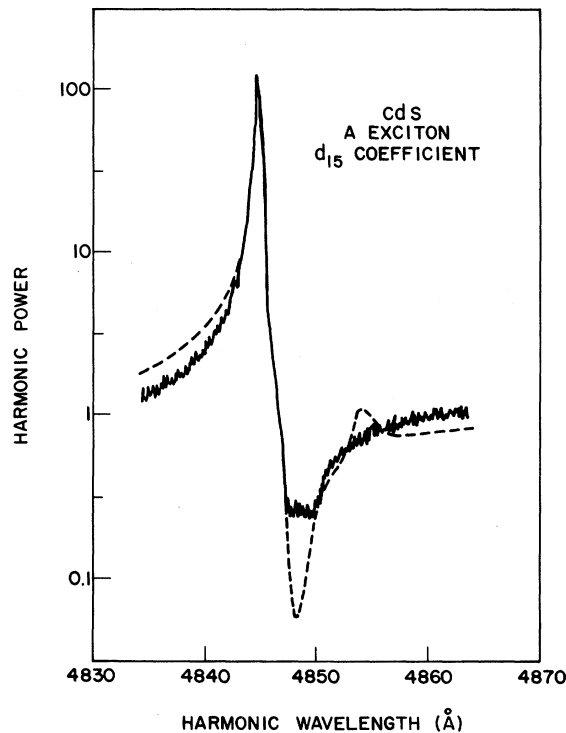


FIG. 9. Comparison showing the good agreement between the experimental resonant second-harmonic power for the CdS *A* exciton (an expanded view of Fig. 2) with a theoretical fit which includes spatial dispersion (dotted line).

the d^{ex} and d^{el} nonlinearities) does not come down far enough towards zero as does that for the *B* exciton. This excess signal is probably due to some background fluorescence at the harmonic wavelength. As can be seen from Figs. 9 and 10, the theoretical fit is quite good. The slight bump in the theoretical curve near ω_0 is not simply a result of spatial dispersion, and in fact, a very similar structure appears in the classical curve (although owing to the scale in Fig. 5 it is not evident). This feature is caused by the near cancellation between the resonantly increasing linear and nonlinear susceptibilities. That is, Eqs. (8) and (20) [or Eqs. (2) and (5)] show that as ω increases and approaches ω_0 both $n(\omega)$ and $d_{ijk}(\omega)$ increase strongly. However, these increases have opposing effects on $I_{\text{shg}}(\omega)$ as can be seen from Eq. (33) [or more clearly from Eq. (6)], resulting in a weak structure near ω_0 . This is discussed more fully in the discussion Sec. VI.

C. Nonlinear susceptibility—ZnO

All the ZnO platelets we investigated had as-grown surfaces and exhibited a significant amount of background fluorescence near the *A*-exciton frequency. This background varied from sample to sample, and the data shown in Fig. 4 are for the best sample having the least fluorescence. Because this background masks the harmonic minimum (see Figs. 9 and 10 for comparison), our

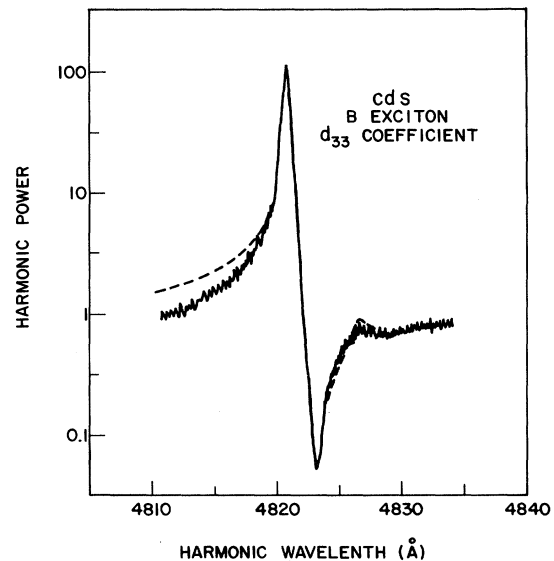


FIG. 10. Comparison of the experimental resonant second-harmonic power for the CdS *B* exciton with a theoretical fit which includes spatial dispersion. Note the good agreement in contrast to the poor classical fit shown in Fig. 5.

TABLE II. Comparison of experimental exciton contributions to the nonlinear coefficient d_{ijk} and those calculated theoretically using the classical or spatial dispersion values for the exciton linear polarizability α . The experimental and calculated ratios of the A - and B -exciton nonlinear coefficients in CdS are also given.

Crystal-exciton	d_{ijk} (sign)	$10^3(d^{ex}/d^{el})$ (expt.)	$10^3(4\pi\alpha^{ex})$ (classical)	$10^3(d^{ex}/d^{el})$ (calc. class.)	$10^3(4\pi\alpha^{ex})$ (sp. disp.)	$10^3(d^{ex}/d^{el})$ (calc. sp. disp.)
CdS - A	$d_{113}(-)$	+3.0	9.4	+4.4	12.5	+5.9
CdS - B	$d_{333}(+)$	+1.7	5.6	+2.6	7.5	+3.5
ZnO - A	$d_{113}(+)$	$\sim +2$	7	+3		
CdS - (B/A)		Experimental ratio	Theoretical ratio			
			$(\alpha_B^{ex}/\alpha_A^{ex})$			
		$\frac{(d_{333}^{ex}/d_{333}^{el})B}{(d_{113}^{ex}/d_{113}^{el})A}$	+0.57		+0.60	

experimental fit to obtain d^{ex} was significantly less accurate than our determinations of d^{ex} for the CdS excitons. The experimental value for d^{ex} (ZnO) given in Table II is probably only accurate to within a factor of ~ 2 . However, it is in agreement with the theoretical prediction to within this experimental error.

VI. DISCUSSION

As mentioned in the Introduction, a simple theory¹¹ for the exciton nonlinearity, namely

$$d_{ijk}^{ex} = 4(4\pi\alpha_{ii}/\epsilon) d_{ijk}^{el}, \quad (43)$$

has successfully explained the selection rules, magnitude, and sign of d_{ijk}^{ex} for CuCl and ZnO. However, both of these crystals are unusual. CuCl has a negative nonlinearity ($d_{123} < 0$) as a result of the Cu d electrons,¹⁷ while ZnO has a negative coefficient ($d_{333} < 0$) caused by the large difference in the covalent radii¹⁷ of Zn and O. Thus, we wanted to measure a more typical nonlinear crystal such as CdS.

The predictions of Eq. (43) are compared with our measurements of d_{ijk}^{ex} (CdS) in Table II. For completeness we have evaluated Eq. (43) using both the classical and spatial dispersion values of the linear exciton polarizability α . Note that the signs of d_{ijk}^{ex} are predicted correctly, i.e., d_{113}^{ex} (CdS) < 0 while d_{333}^{ex} (CdS) > 0 , which are exactly the same signs as the corresponding electronic nonlinearities. It is also noteworthy that the nonlinear coefficient of the CdS B exciton is less than that of the A exciton as further predicted by Eq. (43). As shown in the bottom of Table II, the experimental CdS ratio $(d^{ex}/d^{el})_B/(d^{ex}/d^{el})_A$ is in good agreement with the ratio of linear polarizabilities α for both the clas-

sical and spatial dispersion values. The actual magnitude of the measured nonlinear coefficients, d_{ijk}^{ex} (CdS) seems to be in somewhat better agreement with the theoretical prediction using the classical value of α . This result does not seem unreasonable since the derivation¹¹ of Eq. (43) uses a classical argument which neglects spatial dispersion, and thus it may be more consistent to use the classical polarizability in the theoretical evaluation as was done¹¹ for CuCl and ZnO. However, in either case, the magnitude (and absolute sign) of d_{ijk}^{ex} for the CdS A and B excitons seem well accounted for.

In fact the accuracy of this relationship, Eq. (43), is the reason for the lack of a more pronounced structure in I_{shg} at the resonant frequency ω_0 . This can be seen most simply from the classical expressions as discussed below (but is also true when spatial dispersion is included). At resonance Eqs. (2) and (5) reduce to

$$\epsilon = \epsilon^0 + (4\pi\alpha/\gamma)i \quad (44)$$

$$d = d^{el} + (d^{ex}/\gamma)i, \quad (45)$$

where $\gamma \equiv \Gamma/\omega_0$. Using for simplicity the approximations $4\pi\alpha/\gamma \gg \epsilon^0$, $d^{ex}/\gamma \gg d^{el}$, and $[n(\omega_H) - n(\omega_F)]^2 \ll \kappa^2$ it is easy to show that Eq. (6) for the harmonic intensity at the resonance frequency can be expressed as

$$I_{shg}(\omega_0) \simeq 2(d^{ex}/4\pi\alpha)^2. \quad (46)$$

Far off resonance $\omega \ll \omega_0$ Eqs. (2) and (5) simply reduce to $\epsilon = \epsilon^0$ and $d = d^{el}$. Further using for CdS the experimental result $n_H^0 - n_F^0 = 0.17 n_H^0$ we can write the off-resonance harmonic intensity as

$$I_{shg}(0) \simeq [d^{el}/(0.17)\epsilon^0]^2. \quad (47)$$

Finally we can now estimate the ratio of the harmonic generated at resonance to that generated off resonance as

$$\frac{I_{\text{shg}}(\omega_0)}{I_{\text{shg}}(0)} \approx 2(0.17)^2 \left[\left(\frac{d^{\text{ex}}}{d^{\text{el}}} \right) \left(\frac{\epsilon^0}{4\pi\alpha} \right) \right]^2. \quad (48)$$

The use of the theoretical relation Eq. (43) for d^{ex} gives

$$\frac{I_{\text{shg}}(\omega_0)}{I_{\text{shg}}(0)} \approx 1, \quad (49)$$

showing that the structure near the exciton resonance is expected to be small. In view of the generality of Eq. (43), this should be true for any crystal and also explains, for example, the lack of any strong feature⁶ near the one-photon resonance at ω_0 in CuCl. The structure actually seen in Figs. (4), (9), and (10) is not at ω_0 but is due instead to phase matching and destructive interference between d^{ex} and d^{el} .

VII. SUMMARY AND CONCLUSIONS

We have found that the classical theory gives a very poor fit to our CdS second-harmonic data

(being a factor of ~ 25 too small), which is not really surprising in view of the known^{1,2,5} importance of spatial dispersion in this material. When these spatial dispersion effects are included, the experimental harmonic measurements can be well accounted for, and the magnitude and sign of the exciton nonlinearity d_{ijk}^{ex} can be determined. The theoretical fit to the data uses the same linear exciton parameters as is obtained from reflectivity measurements^{1,2} and checked by our Maker fringe determinations. We found that the selection rules, the magnitude, and the absolute sign of these d_{ijk}^{ex} for CdS and ZnO found in this study are in good agreement with those predicted theoretically,¹¹ and that Kleinman symmetry¹³ is strongly violated as would be expected^{14,15} so close to a resonance.

ACKNOWLEDGMENTS

It is a pleasure to acknowledge interesting comments by J. J. Hopfield. We are also grateful for the excellent CdS crystals which were grown by K. Nassau, and for linear reflectivity measurements by J. P. van der Ziel.

¹J. J. Hopfield and D. G. Thomas, Phys. Rev. **132**, 563 (1963).

²G. D. Mahan and J. J. Hopfield, Phys. Rev. **135**, A428 (1964).

³V. M. Agranovich and V. L. Ginzburg, *Spatial Dispersion in Crystal Optics and the Theory of Excitons* (Interscience, New York, 1966).

⁴D. D. Sell, S. E. Stokowski, R. Dingle, and J. V. DiLorenzo, Phys. Rev. B **7**, 4568 (1973).

⁵F. Evangelisti, A. Frova, and F. Patella, Phys. Rev. B **10**, 4253 (1974).

⁶D. C. Haueisen and H. Mahr, Phys. Rev. B **8**, 734 (1973).

⁷S. D. Kramer, F. G. Parsons, and N. Bloembergen, Phys. Rev. B **9**, 1853 (1974); S. D. Kramer and N. Bloembergen, in *Proceedings of the International Conference on Highly Transparent Media* (Plenum, New York, 1975).

⁸J. Ringeissen, A. Coret, S. Nikitine, in *Localized*

Excitations in Solids, edited by R. F. Wallis (Plenum, New York, 1968).

⁹D. G. Thomas, J. Phys. Chem. Solids **15**, 86 (1959).

¹⁰R. C. Miller and W. A. Nordland, Jr., Phys. Rev. B **2**, 4896 (1970).

¹¹B. F. Levine, Phys. Rev. Lett. **33**, 368 (1974).

¹²J. Jerphagnon and S. K. Kurtz, J. Appl. Phys. **41**, 1667 (1970).

¹³D. A. Kleinman, Phys. Rev. **126**, 1977 (1962).

¹⁴B. F. Levine, IEEE J. Quantum Electron. **QE-9**, 946 (1973).

¹⁵M. D. Levenson and N. Bloembergen, Phys. Rev. B **10**, 4447 (1974).

¹⁶For an excellent discussion of general boundary conditions, see J. J. Hopfield, J. Phys. Soc. Jpn. Suppl. **21**, 77 (1966).

¹⁷B. F. Levine, Phys. Rev. B **7**, 2600 (1973); **10**, 1655 (1974).